Crystal structure and phonon instability of high-temperature β-$Ca(BH_4)_2$

Young-Su Lee, Yoonyoung Kim, and Young Whan Cho
Materials Science and Technology Research Division, Korea Institute of Science and Technology, Seoul 136-791, Republic of Korea

Daniel Shapiro and Chris Wolverton
Department of Materials Science and Engineering, Northwestern University, Evanston, Illinois 60208, USA

Vidvuds Ozoliņš
Department of Materials Science and Engineering, University of California, Los Angeles, California 90095-1595, USA
(Received 26 November 2008; revised manuscript received 7 February 2009; published 13 March 2009)

$Ca(BH_4)_2$ is an interesting candidate for high-density hydrogen storage since it contains a large amount of hydrogen by weight and volume, and has been shown to reversibly release and absorb hydrogen, albeit at moderately high temperatures. $Ca(BH_4)_2$ undergoes a polymorphic transformation around 400–440 K from a low-temperature α-$Ca(BH_4)_2$ phase to a high-temperature β-$Ca(BH_4)_2$ phase. The crystal structure of β-$Ca(BH_4)_2$ has only recently been resolved, and its thermodynamic phase stability is still not well understood. Using a combined experimental and theoretical approach, we have independently determined the structure of β-$Ca(BH_4)_2$ and assessed its thermodynamic stability in the quasiharmonic approximation. The space-group $P4_2/m$ gives an excellent agreement between experiment and theory, confirming the result of a recent study [Buchter *et al.*, J. Phys. Chem. B **112**, 8042 (2008)]. Using density-functional theory (DFT), we obtained a value of 10.9 kJ/mol for the static total-energy difference between the β-$Ca(BH_4)_2$ and the α-$Ca(BH_4)_2$ phases at $T=0$ K (without vibrations). Using DFT linear-response calculations, we find that the $[\frac{1}{2}\frac{1}{2}\xi]$ acoustic phonon branch of β-$Ca(BH_4)_2$ is dynamically unstable on the Brillouin-zone boundary at the $T=0$ K lattice parameters predicted from *static* DFT calculations. This phonon branch is very sensitive to the lattice parameters and can be stabilized by including lattice expansion due to zero-point vibrational contributions in the quasiharmonic approximation. This expanded stable β-$Ca(BH_4)_2$ structure has a room-temperature vibrational entropy that is 16 J/mol K higher than that of the α-$Ca(BH_4)_2$ phase, qualitatively consistent with the observed stabilization of the former at elevated temperatures. The main contribution to the entropy difference between the α-$Ca(BH_4)_2$ and β-$Ca(BH_4)_2$ phases comes from the low-frequency region dominated by translational and rotational phonon modes.

DOI: 10.1103/PhysRevB.79.104107 PACS number(s): 61.66.Fn, 63.20.D−, 71.15.Nc

I. INTRODUCTION

Hydrogen storage properties of metal borohydrides have recently become the subject of active research because these materials have high theoretical storage capacities by both weight and volume. In comparison with the alkali and rare-earth alanates, the lighter BH_4^- unit in borohydrides offers higher capacity but its high thermal stability often requires high temperatures for decomposition, and hence currently limits the practical hydrogen storage applications of borohydrides. According to recent experimental and theoretical findings, $Ca(BH_4)_2$ releases hydrogen at a lower temperature[1–3] than the more extensively studied $LiBH_4$ compound.[4,5] The theoretical hydrogen capacity of $Ca(BH_4)_2$ is 9.6 wt % for the following reaction pathway:

$$Ca(BH_4)_2 \rightarrow \frac{1}{3}CaB_6 + \frac{2}{3}CaH_2 + \frac{10}{3}H_2. \quad (1)$$

The reversibility of this reaction has been demonstrated recently: the formation of $Ca(BH_4)_2$ has been independently confirmed by hydrogenating a mixture of CaB_6 and CaH_2,[6] as well as dehydrogenated $Ca(BH_4)_2$ itself.[7,8]

$Ca(BH_4)_2$ undergoes several polymorphic phase transformations[3,9,10] but the polymorphic crystal structures and relative phase stabilities are still not fully understood. The structure of the low-temperature α-$Ca(BH_4)_2$ phase was resolved by Miwa *et al.*,[1] who assigned it to the face-centered orthorhombic *Fddd* symmetry group. Subsequent first-principles density-functional theory (DFT) calculations confirmed that *Fddd* was the lowest-energy structure among 28 AB_2C_8-type candidate structures from the inorganic crystal structure database (ICSD).[11] Recently, Buchter *et al.*[12] resolved the structure of the high-temperature β-$Ca(BH_4)_2$ phase; they assigned it the space-group $P4_2/m$. Another polymorph designated γ-$Ca(BH_4)_2$ has also been observed at room temperature.[12–14] The space group of γ-$Ca(BH_4)_2$ has been reported as *Pbca*,[12] but there have been no reports to date of the full crystal structure for this phase. Upon increasing temperature, α-$Ca(BH_4)_2$ undergoes a transformation to β-$Ca(BH_4)_2$ in the temperature interval between 400 and 440 K (Refs. 6, 7, and 9); γ-$Ca(BH_4)_2$ also transforms to β-$Ca(BH_4)_2$ but the transition temperature appears to be higher.[13]

A quantitative knowledge of the relative stability of the different polymorphs of $Ca(BH_4)_2$ is key to a full understanding of the thermodynamics and kinetics of hydrogen release from this material. However, such understanding is currently lacking. Here, we utilize a combined experimental and theoretical approach to identify the structure and thermal

stability of the high-temperature β-$Ca(BH_4)_2$ phase. We independently find the crystal structure using a combined approach involving first-principles DFT calculations and Rietveld refinement of experimental x-ray data. In agreement with the results of a previous study,[12] we find that the crystal structure of β-$Ca(BH_4)_2$ is $P4_2/m$. The static DFT total-energy difference at $T=0$ K (without vibrations) between the β-$Ca(BH_4)_2$ and α-$Ca(BH_4)_2$ phases is 10.9 kJ/mol. The previous study by Buchter *et al.*[12] found the enthalpy difference to be about 0.15 eV but free energies, vibrational spectra, and the polymorphic phase transformation were not discussed in detail. Therefore, here we focus more on the finite-temperature thermodynamic properties and the vibrational modes of the two phases. Surprisingly, DFT linear-response calculations show that the zone-boundary $[\frac{1}{2}\frac{1}{2}\xi]$ acoustic phonon branch is dynamically unstable at the static $T=0$ K lattice parameters of β-$Ca(BH_4)_2$. However, this phonon branch can be stabilized by including zero-point vibrational effects on the equilibrium lattice parameter in the quasiharmonic approximation. Our DFT calculations (static total-energy and quasiharmonic phonon contributions) indicate that the room-temperature vibrational entropy of the high-temperature β-$Ca(BH_4)_2$ is 16 J/mol K higher than that of the α-$Ca(BH_4)_2$ phase, qualitatively consistent with the observed stabilization of the former at elevated temperatures.

II. METHODS

A. Experiments

The starting material was $Ca(BH_4)_2 \cdot 2THF$ (assay ca. 98%, Aldrich). Adduct-free β-$Ca(BH_4)_2$ was prepared by drying the as-purchased powder overnight under vacuum at 500 K and subsequently quenching it to room temperature. X-ray diffraction (XRD) data was collected by Bruker D8 advance diffractometer (Cu K_α). The phase composition of the dried powder and crystal structure of β-$Ca(BH_4)_2$ were analyzed using the Rietveld refinement method with TOPAS 4.1.[15]

B. First-principles calculations

The total energies of the candidate $Ca(BH_4)_2$ structures were computed within DFT,[16,17] as implemented in the highly efficient Vienna *Ab Initio* Simulation Package (VASP).[18] Core-valence interactions were described using projector augmented wave (PAW) potentials,[19] and electronic exchange and correlation were treated using the generalized gradient approximation (GGA) of Perdew and Wang.[20] More specifically, we used the Ca_sv, B_h, and H_h potentials from the standard pseudopotential library of VASP, with 3*s* and 3*p* semicore states treated as valence for Ca, and using the "hard" B and H potentials. We used a plane-wave basis cutoff energy of 875 eV and Monkhorst–Pack *k*-point meshes of $4\times4\times4$ or better for all structures. All structural degrees of freedom (atomic positions, cell shapes, and cell volumes) were optimized using the calculated forces and stresses within the constraints of the space group of the prototype structure. We used a set of candidate crystal structures (largely taken from the ICSD) for compounds of stoichiometry AB_2C_8, where C=H/D, F, Cl, Br, I, and O. Details of the calculations and the set of 93 candidate structures can be found in Ref. 21. We considered structures to be equivalent when two different relaxed calculations gave configurations that possessed identical Pearson symbols and degenerate energies (within 1 kJ/mol formula unit).

We performed phonon calculations using density-functional perturbation theory (DFPT) (Ref. 22) as implemented in QUANTUM-ESPRESSO (QE).[23] Helmholtz free energies of α-$Ca(BH_4)_2$ and β-$Ca(BH_4)_2$ were evaluated in the harmonic approximation using phonon density-of-states (PDOS) curves. We use ultrasoft Vanderbilt pseudopotentials[24] and the GGA of Perdew-Burke-Ernzerhof[25] for the DFPT calculations. All atomic species were treated using the same valence electron configurations as in our VASP calculations. The numerical differences with the VASP calculations were found to be minor: the DFT total-energy difference between the α-$Ca(BH_4)_2$ and β-$Ca(BH_4)_2$ phases differed by less than 1 kJ/mol formula unit. We used a plane-wave basis cutoff energy of 680 eV and Monkhorst-Pack *k*-point meshes of $3\times2\times2$ and $2\times2\times4$ for α-$Ca(BH_4)_2$ and β-$Ca(BH_4)_2$, respectively. The interatomic force constants were calculated from dynamical matrices obtained on a uniform $3\times3\times3$ grid of phonon wave vectors. The phonon frequencies at arbitrary **q** vector were then calculated from those interatomic force constants. Phonon densities of states were obtained by integrating over $20\times20\times20$ and $20\times20\times30$ regular meshes for α-$Ca(BH_4)_2$ and β-$Ca(BH_4)_2$, respectively.

III. RESULTS AND DISCUSSION

A. $Ca(BH_4)_2$: crystal structures

Here, we describe how we used a combined experimental/computational approach to deduce the crystal structure of β-$Ca(BH_4)_2$. The observed XRD pattern for our sample containing β-$Ca(BH_4)_2$ is shown in Fig. 1. As a first step in trying to identify the crystal structure, we performed an extensive search for low-energy polymorphs by computing DFT energetics for $Ca(BH_4)_2$ in 93 AB_2C_8 structures. The prototype structures and their fully relaxed DFT total energies are summarized in Table I. Our DFT calculations correctly confirm that the orthorhombic *Fddd* structure of $BaMn_2O_{8-}2$ has the lowest energy among the considered candidate structures of $Ca(BH_4)_2$.[1,11] We simulated XRD patterns of the low-energy structures of Table I, but none of the structures within 10 kJ/mol of the ground-state phase give XRD patterns that resemble the experimental data in Fig. 1.

However, by extending the search window to slightly higher energy polymorphs, we found that two monoclinic structures, $ZnAu_2F_8$ and $CuAl_2Cl_{8-}1$, have major XRD peak positions similar to the experimental ones. These two structures share a common backbone of Ca cations, which forms a slightly distorted body-centered tetragonal lattice. Rietveld refinement of these structures to the XRD pattern in Fig. 1 gives monoclinic angles β that are very close to 90°, suggesting that the structure of β-$Ca(BH_4)_2$ is likely to be tetragonal. Armed with the Ca backbone and symmetry, we performed geometry optimizations of several tetragonal

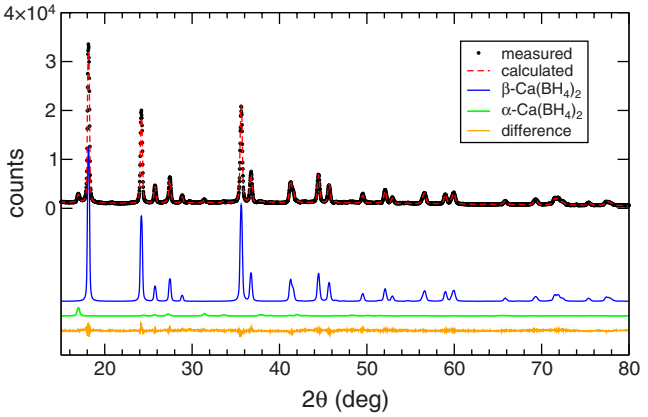

FIG. 1. (Color online) XRD pattern of adduct-free $Ca(BH_4)_2$. The final product is a mixture of 94 wt % β-$Ca(BH_4)_2$ and 6 wt % α-$Ca(BH_4)_2$. The black dots are the measured data and the dashed red (dashed gray) line is the best fit obtained from the Rietveld refinement. The orange (light gray) line at the bottom shows the difference between the measured and calculated patterns. The blue (dark gray) line is the diffraction pattern of β-$Ca(BH_4)_2$; the green (gray) line is for α-$Ca(BH_4)_2$.

structures having different arrangements of four BH_4^- units with fixed Ca positions. Among those, we found that the DFT lattice parameters of the crystal structure of the $P4_2/m$ space group perfectly match with the experimental values. Moreover, this structure is energetically more stable than the two initial candidates, $ZnAu_2F_8$ and $CuAl_2Cl_8$_1. Experimental and theoretical lattice parameters and atomic positions are summarized in Table II, and the structure is shown in Fig. 2 together with the structure of α-$Ca(BH_4)_2$.

To compare with our theoretical predictions, we have analyzed the XRD pattern of the adduct-free powder using the Rietveld refinement method. The powder consists mostly of β-$Ca(BH_4)_2$ and ca. 6 wt % of α-$Ca(BH_4)_2$. There are a few unassigned peaks showing very weak intensities. The Rietveld-refined parameters are summarized together with the DFT-calculated values in Table II. The ability to resolve hydrogen positions from laboratory XRD data is quite limited, and to suppress the error coming from this uncertainty, the following constraints were applied during the refinement procedure. In case of the minor phase α-$Ca(BH_4)_2$, atomic coordinates were fixed to the calculated ones and the anisotropic atomic displacement parameters were fixed to the calculated values in Table III. For β-$Ca(BH_4)_2$, BH_4^- groups were treated as ideal tetrahedra and only the B-H bond length was refined.[26,27] Anisotropic displacement parameters (U_{ij}'s) of Ca were refined but those of B and H were fixed to the calculated values. The refined B-H bond length is 1.016(9) Å and the equivalent isotropic displacement parameter B_{iso} of Ca is 1.5. The refinement process will be discussed in more detail in the next section. In general, the calculated XRD pattern from the present β-$Ca(BH_4)_2$ structure agrees well with the measured one. The weighted pattern R factor (R_{wp}) is 6.0%.

B. Vibrational properties

Interestingly, as shown in Table I, several ICSD structures have lower DFT T=0 K total energies than the presently proposed β-$Ca(BH_4)_2$ structure. This fact raises the possibility that finite-temperature thermodynamic considerations may be responsible for the stabilization of the β-$Ca(BH_4)_2$ phase. In order to investigate the finite-temperature thermodynamics and structural stability of β-$Ca(BH_4)_2$, we have carried out an extensive study of the vibrational free-energy contributions using DFT linear-response calculations of the

TABLE I. Energetics and Pearson symbols for $Ca(BH_4)_2$ calculated in each of the structures in our database of 93 AB_2C_8 compounds. Energies are given in kJ/mol formula unit, relative to the lowest-energy $BaMn_2O_8$_2-type structure. Results are shown for distinct structures having total energies within 100 kJ/mol of the ground-state energy. Structures with identical Pearson symbols and relaxed energies within 1 kJ/mol per formula unit were considered equivalent. Note that in the Pearson symbols, we list the number of atoms in the primitive unit cell rather than the conventional unit cell.

Structure	Energy	Pearson symbol
$BaMn_2O_8$_2	0.00	oF22
$TiAl_2Br_8$_2	1.39	mC22
$BaAl_2Cl_8$	1.63	mP22
$ZrMo_2O_8$_1	2.09	hP66
$TiAl_2Cl_8$_2	3.24	mC22
β-$Ca(BH_4)_2$	10.90	tP22
$ZnAu_2F_8$	13.92	mP22
$HfMo_2O_8$_1	18.53	hP66
$CuAl_2Cl_8$_1	19.46	mP22
$CaAl_2Cl_8$	20.23	tI44
$CdAl_2Cl_8$_2	20.66	mP22
$SrAl_2Cl_8$_1	21.52	tI44
$SrAl_2Cl_8$_2	21.89	oP88
BeB_2H_8	22.15	tI88
$PdAu_2F_8$	22.61	mP22
BaB_2F_8	24.71	mP88
$ThMo_2O_8$_4	25.26	hP99
$ZrMo_2O_8$_2	25.95	mP22
$ZrMo_2O_8$_3	33.61	oP22
$TiAl_2Br_8$_1	34.78	oP22
$NiCl_2O_8$	35.03	hR11
$ThMo_2O_8$_1	35.23	hP66
CaB_2F_8	35.51	oP88
$BaAu_2F_8$	40.69	tI22
$PdGa_2Br_8$	40.92	mC11
UI_2O_8	44.96	mP22
ZrW_2O_8_1	47.77	cP44
ZrS_2O_8	55.69	oP44
UMo_2O_8_1	56.65	hP99
$PdGa_2I_8$	67.68	mC11
$PbRe_2O_8$	69.59	hP33
$ZrMo_2O_8$_4	69.89	mC11
$ThMo_2O_8$_2	79.72	hP99
$BaMn_2O_8$_1	81.37	oF22

TABLE II. DFT-calculated (from QE) and experimental (Rietveld-refined) crystal structures of β-$Ca(BH_4)_2$ and α-$Ca(BH_4)_2$.

	Lattice parameter (Å)	Atom	Wyckoff positions	x	y	z
Calculated						
β-$Ca(BH_4)_2$	a=6.930	Ca	2d	0.0000	0.5000	0.5000
	c=4.358	B	4j	0.2038	0.6837	0.0000
	V=104.6 Å^3/f.u.	H1	4j	0.3796	0.6922	0.0000
		H2	4j	0.1709	0.5097	0.0000
		H3	8k	0.1359	0.7630	0.7732
α-$Ca(BH_4)_2$	a=8.745	Ca	8a	0.0000	0.0000	0.0000
	b=13.105	B	16f	0.0000	0.2219	0.0000
	c=7.495	H1	32h	−0.1129	0.2763	0.0108
	V=107.4 Å^3/f.u.	H2	32h	−0.0002	0.1687	0.1353
Experimental[a]						
β-$Ca(BH_4)_2$ [b]	a=6.9241(2)	Ca	2d	0.000	0.500	0.500
	c=4.3492(1)	B	4j	0.210(2)	0.695(2)	0.000
	V=104.3 Å^3/f.u.	H1	4j	0.363	0.680	0.000
		H2	4j	0.163	0.548	0.000
		H3	8k	0.170	0.755	0.809
α-$Ca(BH_4)_2$	a=8.772(6)					
	b=13.118(7)					
	c=7.496(4)					
	V=107.8 Å^3/f.u.					

[a] R_{wp}=6.0%, goodness of fit=2.5.
[b] R_{Bragg}=2.6%.

harmonic phonon dispersions of α-$Ca(BH_4)_2$ and β-$Ca(BH_4)_2$. To correctly treat phonons in polar crystals, the electronic dielectric-constant tensor and Born effective charge were calculated within the same framework,[22] and the results are reflected in phonon frequencies. These quantities are summarized in Tables IV and V. The calculated harmonic phonon dispersion of the β-$Ca(BH_4)_2$ phase at the *static* (i.e., without thermal expansion and zero-point corrections) lattice parameters is shown in Fig. 3(a). The low-temperature α-$Ca(BH_4)_2$ structure (not shown in Fig. 3) is predicted to be dynamically stable but the high-temperature β-$Ca(BH_4)_2$ phase shows a more complex behavior: while all the phonon modes are stable at the zone-center Γ point, one of the transverse-acoustic modes becomes unstable at the Brillouin-zone boundary along the $[\frac{1}{2}\frac{1}{2}\xi]$ line, as evidenced by imaginary frequencies in Fig. 3(a).

As can be inferred from the smallness of these imaginary frequencies, the potential-energy profile is extremely flat when the atoms are displaced according to the eigenvector of the unstable mode. This conclusion was confirmed using frozen phonon calculations where the atoms were displaced along the eigenvectors of the unstable mode at the zone-boundary M point; this mode preserves the symmetry of the crystal but leads to a doubling of the unit cell. Using a larger $\sqrt{2}\times\sqrt{2}\times1$ supercell to relax all structural degrees of freedom (including lattice parameters and internal coordinates), we found that the total energy was reduced by only 0.001 kJ/mol when using VASP PAW potentials and GGA, and by 0.01 kJ/mol when using QE ultrasoft pseudopotentials and GGA. These values indicate a very weak driving force for transformation to a bigger unit cell of the same $P4_2/m$ symmetry. Furthermore, frozen phonon calculations within a $\sqrt{2}\times\sqrt{2}\times2$ $P4_2/m$ supercell showed that all the remaining phonon modes are stable after the atomic displacements within the supercell have been allowed to relax to one of the two symmetrical energy minima along the unstable M-point mode eigenvectors. We also find that a rather small (>2%) lattice expansion along the a direction can stabilize the frequencies of the unstable modes. Furthermore, we find that upon lattice expansion, the internal atomic coordinates relax back to the ideal positions of the $1\times1\times1$ $P4_2/m$ structure. Therefore, using the larger $\sqrt{2}\times\sqrt{2}\times1$ supercell, for each set of lattice parameters one can define a crystal structure that has harmonically stable phonons. These phonons can then be used to calculate the harmonic free energy of β-$Ca(BH_4)_2$ as a function of a and c, and apply the quasiharmonic approximation to study thermal-expansion effects.

However, for computational efficiency, we use linear-response calculations on the $1\times1\times1$ unit cell of $P4_2/m$ and presume that the contribution from the unstable mode to the

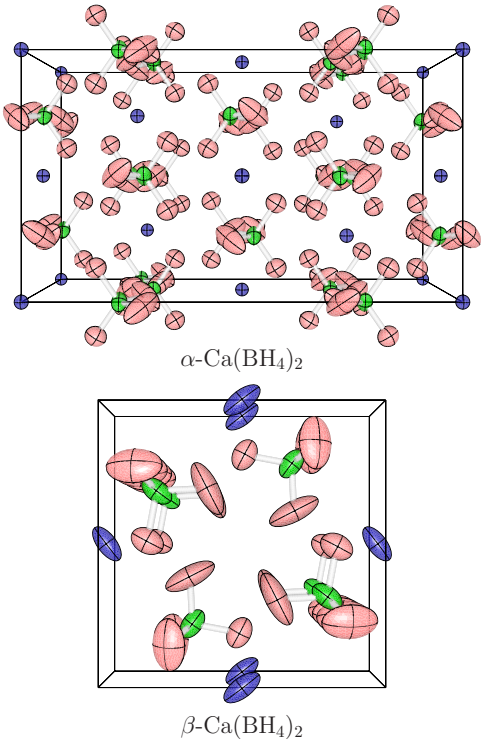

FIG. 2. (Color online) Crystal structures of α-$Ca(BH_4)_2$ (top) and β-$Ca(BH_4)_2$ (bottom). Thermal displacement ellipsoids at 298 K are shown. Ca, B, and H atoms are in blue (dark gray), green (gray), and pink (light gray), respectively.

zero-point energy can be neglected because less than 5% of the lowest-energy phonon branch is unstable at the total-energy minimum. If we assign a harmonic-oscillator frequency of 30 cm^{-1} to this part [this estimate was obtained from the frequency maximum of the unstable mode along the Γ-M line in Fig. 3(b)], the contribution will be at most 0.01 kJ/mol. We start from the total energy of β-$Ca(BH_4)_2$ as a function of $a(=b)$ and c, which is presented in the contour plot of Fig. 4. We note that the structure itself is quite soft; it costs very little in energy to expand, especially along the in-plane a or b directions ($C_{11}=C_{22}=15$ GPa, $C_{33}=52$ GPa). When the zero-point energy is included, the free-energy minimum point at 0 K shifts to ~2% and 1% expansions along a and c, respectively, as shown in the bottom panel of Fig. 4. As found in the frozen phonon calculation, the lowest-energy acoustic mode becomes stable at these expanded lattice parameters: the shaded area in the contour plot covers the points where we find the lowest frequency mode to be unstable but the free-energy minimum point is located outside of this area. The phonon-dispersion curve is presented in Fig. 3(b). From now on, we refer to this expanded dynamically stable structure of Fig. 3(b) as β_{st} and the structure at total-energy minimum as β_0 (annotated in Fig. 4). At 298 K, the lattice expansion along the in-plane a direction is predicted to be more than 3% and deviates noticeably from the experimental values. This discrepancy can be attributed to several possible causes. First, the β-$Ca(BH_4)_2$ structure is very soft and the GGA may simply not be accurate enough to give the correct lattice parameters. However, we are inclined to think that the main reason for this discrepancy lies in a quantitative failure of the quasiharmonic approximation at finite temperatures. Indeed, the free energy at high temperatures is dominated by the vibrational entropy term, which in turn is heavily affected by the lowest phonon frequencies (since it is proportional to the logarithmic moment of the phonon density of states), while the electronic zero-point energy is given by the first moment of the phonon density of states and relatively insensitive to the lowest-energy phonon frequencies. Therefore, a quasiharmonic treatment of the low-energy phonon branches may be quantitatively inaccurate, and intrinsically anharmonic contributions to the finite-temperature free energy could be significant. For instance, it is known that the high-temperature structure of $LiBH_4$ has several harmonically unstable phonon branches,[28,29] and anharmonic effects of BH_4^- motion or even static or dynamic

TABLE IV. Electronic dielectric-constant tensor ϵ_∞ of β-$Ca(BH_4)_2$ and α-$Ca(BH_4)_2$. The off-diagonal components are zero.

	$\epsilon_{\infty,11}$	$\epsilon_{\infty,22}$	$\epsilon_{\infty,33}$
β-$Ca(BH_4)_2$	2.71	2.71	2.86
α-$Ca(BH_4)_2$	2.77	2.72	2.62

TABLE III. DFT-calculated anisotropic and isotropic atomic displacement parameters of the structures, β_0, and α-$Ca(BH_4)_2$. The unstable modes of β_0 are not considered in the calculation. The B_{iso} values inside parenthesis are those of β_{st}. Units are $Å^2$.

	Atom	U_{11}	U_{22}	U_{33}	U_{12}	U_{13}	U_{23}	B_{iso}
β-$Ca(BH_4)_2$	Ca	0.057	0.082	0.018	−0.043	0	0	4.1(2.9)
	B	0.056	0.042	0.021	−0.022	0	0	3.1(2.9)
	H1	0.066	0.166	0.158	−0.070	0	0	10.3(9.2)
	H2	0.063	0.045	0.060	−0.014	0	0	4.4(4.1)
	H3	0.188	0.072	0.046	0.004	−0.029	0.014	8.1(7.2)
α-$Ca(BH_4)_2$	Ca	0.017	0.018	0.018	0	0	0	1.4
	B	0.033	0.022	0.036	0	−0.018	0	2.4
	H1	0.101	0.093	0.079	0.068	−0.053	−0.042	7.2
	H2	0.055	0.042	0.039	−0.001	−0.002	0.004	3.6

TABLE V. Born effective charge tensor $\mathbf{Z}^*$ of each ionic specie in β-$Ca(BH_4)_2$ and α-$Ca(BH_4)_2$.

	Atom	$\frac{1}{3}\mathrm{Tr}(\mathbf{Z}^*)$	Z^*_{11}	Z^*_{22}	Z^*_{33}	Z^*_{12}	Z^*_{21}	Z^*_{13}	Z^*_{31}	Z^*_{23}	Z^*_{32}
β-$Ca(BH_4)_2$	Ca	2.34	2.45	1.98	2.58	−0.03	−0.21	0	0	0	0
	B	0.13	0.18	0.00	0.20	−0.11	0.08	0	0	0	0
	H1	−0.34	−0.63	−0.22	−0.17	−0.18	−0.28	0	0	0	0
	H2	−0.32	−0.19	−0.48	−0.31	−0.22	−0.18	0	0	0	0
	H3	−0.32	−0.25	−0.20	−0.51	−0.02	−0.05	−0.18	−0.20	0.04	0.08
α-$Ca(BH_4)_2$	Ca	2.28	2.42	2.31	2.10	0	0	0	0	0	0
	B	0.17	0.18	0.17	0.16	0	0	−0.02	0.07	0	0
	H1	−0.32	−0.51	−0.25	−0.20	0.20	0.19	−0.12	−0.21	0.01	0.05
	H2	−0.33	−0.19	−0.41	−0.41	−0.00	−0.03	−0.14	−0.12	0.17	0.15

disorder of BH_4^- need to be accounted to explain the stabilization of this harmonically unstable structure.[30,31]

While again a fully anharmonic calculation would be necessary to accurately treat the frequency and free-energy contributions arising from harmonically unstable modes, we have tried to estimate the α-$Ca(BH_4)_2$ to β-$Ca(BH_4)_2$ transition temperature within the limitation of the quasiharmonic approximation. Figure 5 compares the calculated PDOS of α-$Ca(BH_4)_2$ and β-$Ca(BH_4)_2$. It is worth noting that both the experimental and theoretical results agree that the molar volume of β-$Ca(BH_4)_2$ is 3% smaller than that of α-$Ca(BH_4)_2$, which implies that atoms in β-$Ca(BH_4)_2$ are relatively tightly bound, and the phonon frequencies of β-$Ca(BH_4)_2$ could be expected to be lower than those of α-$Ca(BH_4)_2$. Contrary to the intuitive considerations that lower-volume phases should have higher vibrational frequencies, we find that the low-energy modes of β-$Ca(BH_4)_2$ are downshifted relative to α-$Ca(BH_4)_2$, which is the main reason for thermal stabilization of β-$Ca(BH_4)_2$ at high temperatures. In contrast, the high-energy modes, which involve bending and stretching deformations of B-H bonds, do not contribute significantly to the entropy since the typical energies required to activate these modes (1000 cm^{-1}=1439 K) are not available at the experimental transition temperature of approximately 420 K. At T=298 K, the calculated entropies of α-$Ca(BH_4)_2$ and β_{st} phases are 124 and 140 J/mol K, respectively. Using these entropies along with the calculated energies, we obtain a rough prediction of the transition temperature from α-$Ca(BH_4)_2$ to β_{st} of approximately 600 K, which is 150–200 K higher than the experimental value. The fact that DFT predicts that the vibrational entropy is higher in β-$Ca(BH_4)_2$ than in α-$Ca(BH_4)_2$ is in qualitative agreement with the experimental observation that α-$Ca(BH_4)_2$ transforms into β-$Ca(BH_4)_2$ at elevated temperatures but a quantitatively accurate prediction of the transition temperature is still difficult to achieve using state-of-the-art first-principles free energies.

In what follows, we analyze the effects of the low-frequency vibrational modes on the atomic displacements in α-$Ca(BH_4)_2$ and β-$Ca(BH_4)_2$. We consider the anisotropic displacement tensor $\mathbf{U}$, which for an atomic specie α is defined as

$$U_{ij,\alpha} = \frac{1}{N_{\mathbf{q}}} \sum_{n,\mathbf{q}} \frac{\hbar}{\omega_{n\mathbf{q}}} \frac{e^{i,\alpha}_{n\mathbf{q}} (e^{j,\alpha}_{n\mathbf{q}})^*}{M_\alpha} \left[\frac{1}{2} \coth \frac{\hbar \omega_{n\mathbf{q}}}{2k_B T} \right], \tag{2}$$

where $\omega_{n\mathbf{q}}$ is the vibrational frequency of n_{th} phonon branch at wave vector $\mathbf{q}$, $\mathbf{e}^{\alpha}_{n\mathbf{q}}$ is the normalized eigenvector of the corresponding vibrational mode, M_α is the atomic mass, and $N_{\mathbf{q}}$ is the number of sampled $\mathbf{q}$ vectors.[32] For comparison with experimental studies, we also calculate the equivalent isotropic displacement parameter B_{iso} (Ref. 33):

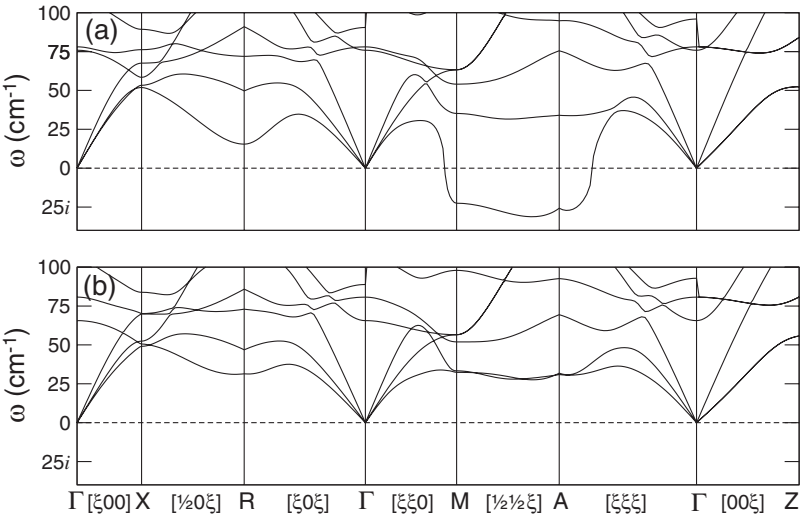

FIG. 3. Phonon dispersion of β-$Ca(BH_4)_2$ along the seven lines in Brillouin zone. Γ is the origin of the Brillouin zone. High symmetry points denoted by Roman letters are X:$(\frac{1}{2}00)$, R:$(\frac{1}{2}0\frac{1}{2})$, M:$(\frac{1}{2}\frac{1}{2}0)$, A:$(\frac{1}{2}\frac{1}{2}\frac{1}{2})$, and Z:$(00\frac{1}{2})$. ξ runs either from 0 to $\frac{1}{2}$ or from $\frac{1}{2}$ to 0. Frequencies below ω=0 line correspond to imaginary frequencies. (a) At total-energy minimum (henceforth referred to as β_0); (b) 2% elongation along a and b, and 1% along c from β_0. Note that the instability vanishes for this stable expanded geometry, which we refer to as β_{st}.

$$B_{\mathrm{iso}} = 8\pi^2 \frac{1}{3} \mathrm{Tr}(\mathbf{U}). \quad (3)$$

The results are summarized in Table III and the thermal displacement ellipsoids are shown in Fig. 2. The most notable change is found in the thermal motion of Ca atom; in α-$Ca(BH_4)_2$, we find almost isotropic motion with small B_{iso}, whereas β-$Ca(BH_4)_2$ shows anisotropic motion with relatively large B_{iso}. U_{ij}'s and B_{iso} of H atoms differ significantly among the symmetrically inequivalent sites. More importantly, the vibrational motions are far from being isotropic, especially in the case of atoms with large B_{iso}. This anisotropy may explain why the Rietveld-refined configurations of BH_4^- units often deviate from the nearly ideal tetrahedral geometries with B-H bond lengths of ca. 1.2 Å, which are predicted by most DFT calculations.[1,28,34,35] Indeed, assigning the same B_{iso} to all H ions should introduce errors into the analysis of the x-ray diffraction data. Confounding the experimental difficulties caused by the weak scattering signal from hydrogen, large anisotropic motions of H ions further complicate the task of obtaining accurate positions of H atoms since U_{ij}'s and atomic coordinates are highly correlated quantities in the standard Rietveld refinement procedure. This large and often anisotropic thermal motion is more conspicuous in the case of high-temperature phases of metal borohydrides, including β-$Ca(BH_4)_2$.[26,36]

The low-frequency phonons that are the main contributors to the atomic displacement tensors represent translational and rotational modes of the Ca cations and BH_4^- complex anions; electrostatic interactions between the H^- and Ca^{2+} ions are the forces controlling the frequencies and atomic displacements of these modes. To further analyze the relationship between the crystal structure and dynamical properties, we calculate the H-Ca distances for each symmetry inequivalent H ion up to the third-nearest-neighbor Ca ion; the results are summarized in Table VI. We find a definite correlation between B_{iso} and H-Ca distances. In both structures, the H1 ions with the highest B_{iso} have very similar Ca coordination environments: one close Ca ion (within 2.35 Å) and two distant Ca ions (beyond 3.6 Å). On the contrary, the H2 ions are bonded by two rather close Ca ions (~2.5 Å) and have small B_{iso}. The H3 ion in β-$Ca(BH_4)_2$ exhibits an intermediate behavior. The Ca ions in α-$Ca(BH_4)_2$ are surrounded by twelve approximately isotropically distributed H atoms, which leads to isotropic vibrations of the Ca ions in α-$Ca(BH_4)_2$. However, the Ca ions in β-$Ca(BH_4)_2$ are coordinated to ten H atoms in an anisotropic fashion, which leads to strongly correlated vibrations of Ca and H1 ions, resulting in very large B_{iso} for both. In going from β_0 to the stable structure β_{st}, B_{iso} of Ca is most strongly affected, indirectly

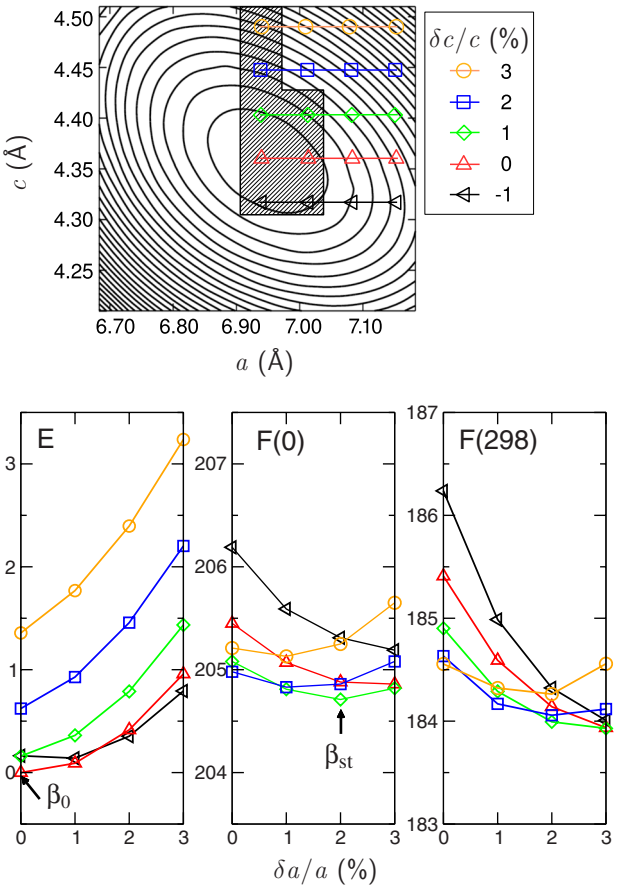

FIG. 4. (Color online) Top: energy of β-$Ca(BH_4)_2$ as a function of lattice parameters $a(=b)$ and c. The contour lines are drawn in 0.2 kJ/mol intervals. The four a and five c values that are used to calculate Helmholtz free energies at finite temperature are marked on top of the contour lines. The points with the same c value are connected by lines and marked with identical symbols; the same convention is used in the bottom panel. The hatched area includes the points where we find imaginary frequency modes. Bottom: DFT total energies and Helmholtz free energies at 0 and 298 K for twenty combinations of a and c values marked on the contour plot in the top panel. The equilibrium lattice parameter at 0 K increases by ca. 2% along a and ca. 1% along c when the zero-point energy is included.

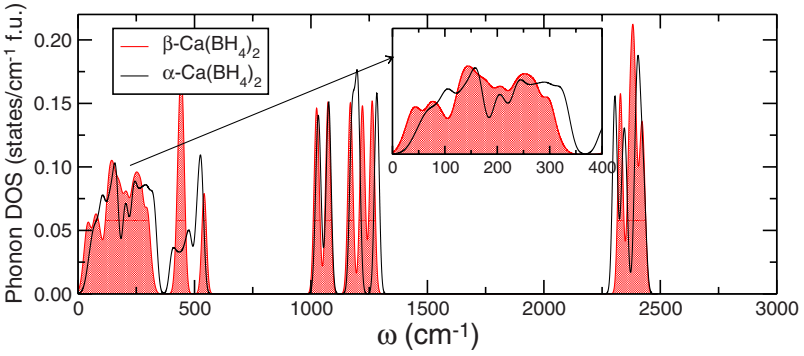

FIG. 5. (Color online) Comparison of the PDOS of β-$Ca(BH_4)_2$ and α-$Ca(BH_4)_2$. PDOS of β-$Ca(BH_4)_2$ is indicated by filled area in red (gray); the black line is for α-$Ca(BH_4)_2$. Low-frequency modes in β-$Ca(BH_4)_2$ are shifted downward compared to those in α-$Ca(BH_4)_2$. Gaussian broadening of 10 cm^{-1} is used.

TABLE VI. H-Ca distances up to the third nearest neighbors in the calculated β-$Ca(BH_4)_2$ and α-$Ca(BH_4)_2$ structures. The numbers inside brackets are multiplicity.

	Bond	Distance (Å)
β-$Ca(BH_4)_2$	H1-Ca	2.291 [1], 3.666 [2], 4.869 [1]
	H2-Ca	2.481 [2], 4.092 [1], 4.205 [1]
	H3-Ca	2.372 [1], 3.169 [1], 3.773 [1]
α-$Ca(BH_4)_2$	H1-Ca	2.320 [1], 3.662 [1], 3.751 [1]
	H2-Ca	2.431 [1], 2.581 [1], 3.777 [1]

showing the importance of Ca motion in the anharmonicity of β-$Ca(BH_4)_2$.

IV. CONCLUSIONS

In conclusion, we have identified the crystal structure of the high-temperature β-$Ca(BH_4)_2$ and analyzed its thermodynamic stability. A combined use of experimental x-ray data, DFT calculations, and Rietveld refinement allowed for the crystal structure determination of this high-temperature polymorph. We find an instability of β-$Ca(BH_4)_2$ when the phonon dispersion is evaluated at the static total-energy minimum geometry; however, the unstable phonon branch becomes stable when the zero-point energy and the associated lattice expansion are considered within the quasiharmonic approximation. Although the thermal expansion can partly deal with the complexity arising from the unstable mode, the presence of the unstable mode may imply that the quasiharmonic approximation could not accurately predict the finite-temperature free energy of β-$Ca(BH_4)_2$. Nonetheless, the quasiharmonic approximation qualitatively predicts the stabilization of β-$Ca(BH_4)_2$ over α-$Ca(BH_4)_2$ as temperature increases. We obtain an estimate of the β-$Ca(BH_4)_2$/α-$Ca(BH_4)_2$ entropy difference at room temperature of 16 J/mol K, which is in reasonable agreement with the observed thermal stability of β-$Ca(BH_4)_2$ at above 440 K.

ACKNOWLEDGMENTS

Y.-S.L., Y.K., and Y.W.C. acknowledge financial support by the KIST Core-Competence Program. V.O., D.S., and C.W. were supported by the U.S. Department of Energy, Office of Science, Basic Energy Sciences under Grant No. DE-FG02-07ER46433.

[1] K. Miwa, M. Aoki, T. Noritake, N. Ohba, Y. Nakamori, S. I. Towata, A. Zuttel, and S. I. Orimo, Phys. Rev. B **74**, 155122 (2006).
[2] D. J. Siegel, C. Wolverton, and V. Ozoliņš, Phys. Rev. B **76**, 134102 (2007).
[3] J.-H. Kim, S.-A. Jin, J.-H. Shim, and Y. W. Cho, J. Alloys Compd. **461**, L20 (2008).
[4] A. Züttel, S. Rentsch, P. Fischer, P. Wenger, P. Sudan, Ph. Mauron, and C. Emmenegger, J. Alloys Compd. **356-357**, 515 (2003).
[5] J. J. Vajo, S. L. Skeith, and F. Mertens, J. Phys. Chem. B **109**, 3719 (2005).
[6] E. Rönnebro and E. Majzoub, J. Phys. Chem. B **111**, 12045 (2007).
[7] J.-H. Kim, S.-A. Jin, J.-H. Shim, and Y. W. Cho, Scr. Mater. **58**, 481 (2008).
[8] J.-H. Kim, J.-H. Shim, and Y. W. Cho, J. Power Sources **181**, 140 (2008).
[9] G. Barkhordarian, T. Jensen, S. Doppiu, U. Bösenberg, A. Borgschulte, R. Gremaud, Y. Cerenius, M. Dornheim, T. Klassen, and R. Bormann, J. Phys. Chem. C **112**, 2743 (2008).
[10] M. Aoki, K. Miwa, T. Noritake, N. Ohba, M. Matsumoto, H.-W. Li, Y. Nakamori, S. Towata, and S. Orimo, Appl. Phys. A: Mater. Sci. Process. **92**, 601 (2008).
[11] P. Vajeeston, P. Ravindran, and H. Fjellvåg, J. Alloys Compd. **446-447**, 44 (2007).
[12] F. Buchter *et al.*, J. Phys. Chem. B **112**, 8042 (2008).
[13] M. D. Riktor, M. H. Sørby, K. Chłopek, M. Fichtner, F. Buchter, A. Züttel, and B. C. Hauback, J. Mater. Chem. **17**, 4939 (2007).
[14] M. Fichtner, K. Chłopek, M. Longhini, and H. Hagemann, J. Phys. Chem. C **112**, 11575 (2008).
[15] TOPAS version 4.1, Bruker AXS, Karlsruhe, Germany, 2003–2008.
[16] P. Hohenberg and W. Kohn, Phys. Rev. **136**, B864 (1964).
[17] W. Kohn and L. J. Sham, Phys. Rev. **140**, A1133 (1965).
[18] G. Kresse and J. Hafner, Phys. Rev. B **47**, 558 (1993).
[19] P. E. Blöchl, Phys. Rev. B **50**, 17953 (1994).
[20] J. P. Perdew and Y. Wang, Phys. Rev. B **45**, 13244 (1992).
[21] C. Wolverton and V. Ozoliņš, Phys. Rev. B **75**, 064101 (2007).
[22] S. Baroni, S. de Gironcoli, A. Dal Corso, and P. Giannozzi, Rev. Mod. Phys. **73**, 515 (2001).
[23] QUANTUM-ESPRESSO is a community project for high-quality quantum-simulation software, based on density-functional theory, and coordinated by Paolo Giannozzi. See http://www.quantum-espresso.org and http://www.pwscf.org.
[24] D. Vanderbilt, Phys. Rev. B **41**, 7892 (1990).
[25] J. P. Perdew, K. Burke, and M. Ernzerhof, Phys. Rev. Lett. **77**, 3865 (1996).
[26] J.-H. Her, P. W. Stephens, Y. Gao, G. L. Soloveichik, J. Rijssenbeek, M. Andrus, and J.-C. Zhao, Acta Crystallogr., Sect. B: Struct. Sci. **63**, 561 (2007).
[27] R. Černý, Y. Filinchuk, H. Hagemann, and K. Yvon, Angew. Chem., Int. Ed. **46**, 5765 (2007).
[28] K. Miwa, N. Ohba, S. I. Towata, Y. Nakamori, and S. I. Orimo, Phys. Rev. B **69**, 245120 (2004).
[29] Z. Łodziana and T. Vegge, Phys. Rev. Lett. **93**, 145501 (2004).
[30] N. A. Zarkevich and D. D. Johnson, Phys. Rev. Lett. **100**, 040602 (2008).
[31] Y. Filinchuk, D. Chernyshov, and R. Cerny, J. Phys. Chem. C **112**, 10579 (2008).

[32] S. Scandolo, P. Giannozzi, C. Cavazzoni, S. de Gironcoli, A. Pasquarello, and S. Baroni, Z. Kristallogr. **220**, 574 (2005).
[33] K. N. Trueblood, H.-B. Bürgi, H. Burzlaff, J. D. Dunitz, C. M. Gramaccioli, H. H. Schulz, U. Shmueli, and S. C. Abrahams, Acta Crystallogr., Sect. A: Found. Crystallogr. **52**, 770 (1996).
[34] J.-Ph. Soulié, G. Renaudin, R. Černý, and K. Yvon, J. Alloys Compd. **346**, 200 (2002).
[35] A. Zuttel, P. Wenger, S. Rentsch, P. Sudan, P. Mauron, and C. Emmenegger, J. Power Sources **118**, 1 (2003).
[36] M. R. Hartman, J. J. Rush, T. J. Udovic, R. C. Bowman, Jr., and S.-J. Hwang, J. Solid State Chem. **180**, 1298 (2007).